nature photonics

LETTERS

PUBLISHED ONLINE: 16 FEBRUARY 2014 | DOI: 10.1038/NPHOTON.2014.9

High-speed plasmonic phase modulators

A. Melikyan[1]*, L. Alloatti[1], A. Muslija[1], D. Hillerkuss[2], P. C. Schindler[1], J. Li[1], R. Palmer[1], D. Korn[1], S. Muehlbrandt[1], D. Van Thourhout[3], B. Chen[4], R. Dinu[4,5], M. Sommer[1], C. Koos[1], M. Kohl[1], W. Freude[1]* and J. Leuthold[1,2]*

To keep pace with the demands in optical communications, electro-optic modulators should feature large bandwidths, operate across all telecommunication windows, offer a small footprint, and allow for CMOS-compatible fabrication to keep costs low[1]. Here, we demonstrate a new ultra-compact plasmonic phase modulator based on the Pockels effect in a nonlinear polymer. The device has a length of only 29 μm and operates at 40 Gbit s^{-1}. Its modulation frequency response is flat up to 65 GHz and beyond. The modulator has been tested to work across a 120-nm-wide wavelength range centred at 1,550 nm, and is expected to work beyond this range. Its operation has been verified for temperatures up to 85 °C and it is easy to fabricate. To the best of our knowledge, this is the most compact high-speed phase modulator demonstrated to date.

High-speed, ultra-compact and power-efficient electro-optic modulators are currently in the spotlight of research as they are key components in optical transmission links[1,2]. To this day, the majority of silicon-based modulators exploit either the plasma dispersion effect in silicon[3–12] or the Pockels effect in nonlinear cladding, a technology also known as silicon–organic hybrid (SOH)[13–15]. The configuration of silicon modulators can be classified as resonant[3–8,14] or non-resonant[9–13,15]. Resonant modulators can be very compact. Indeed, a device with a footprint as small as 78 μm^2 has already been demonstrated[3]. This size is possible due to the large quality factor of the resonant cavity, which enhances the nonlinear interaction by several orders of magnitude. However, resonant modulators suffer from bandwidth limitations and need to be optimized for a certain operating wavelength range. In addition, resonant modulators are sensitive to temperature fluctuations and fabrication tolerances. In contrast, non-resonant modulators offer operation across a large spectral window. They are typically based on a travelling wave configuration. To achieve a long interaction time between the optical and the modulating radiofrequency (RF) signal, these devices are often several millimetres in length, which increases the RF losses of the device. Such bulky dimensions also prevent economically efficient co-integration with electronics. A further disadvantage of the travelling wave approach is the requirement to terminate the RF transmission line with a matched impedance, which reduces the modulating voltage to half the generator's open-circuit voltage.

Surface plasmon photonics or 'plasmonics' is the art of controlling, guiding and detecting surface plasmon polaritons (SPPs). The SPP is an electromagnetic surface wave at a dielectric–metal interface, coupled to the charge density oscillation in the metal surface[16,17]. Plasmonics is a means of providing ultra-compact and high-speed components such as modulators, switches and detectors[18–21]. Since the 1980s, the realization of a plasmonic modulator has been the focus of many research groups[22–29]. Modulation of an SPP with an electrical signal has been shown by employing the thermo-optic effect[22], the Pockels effect[23–25] and the plasma dispersion effect either in semiconductors or in metals[26–29]. However, despite the many approaches pursued in the past 30 years, an electro-optical high-speed plasmonic modulator has never been demonstrated.

Here, we present a plasmonic phase modulator (PPM) that combines the large RF bandwidth of a travelling wave modulator[9–13,15],

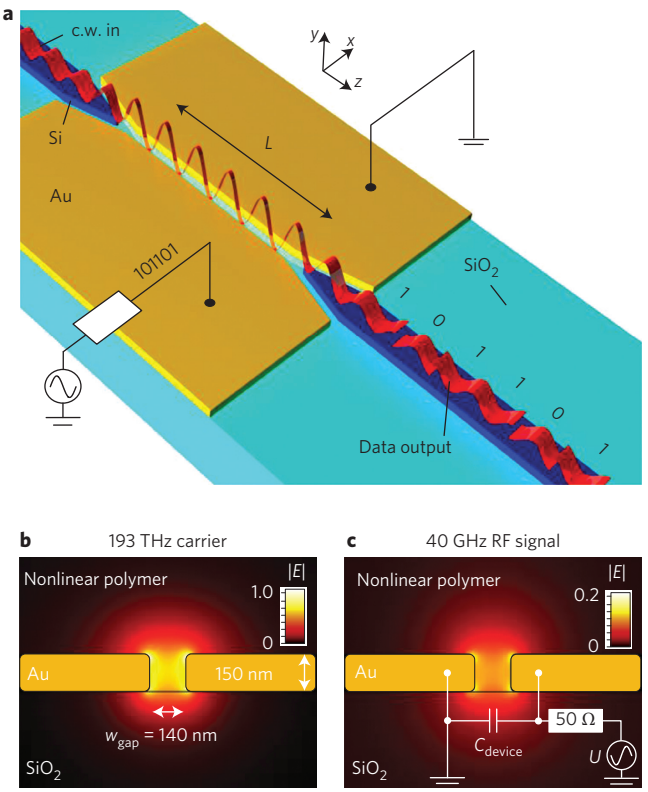

Figure 1 | PPM and field distributions. a, Schematic of the PPM. Continuous-wave (c.w.) infrared light guided by the upper-left silicon nanowire is coupled through a metal taper to the plasmonic slot waveguide. The slot in the metal sheets is filled with an electro-optic polymer. The phase of the surface plasmon polariton (SPP), which propagates in the slot, is changed by applying a modulating voltage. A second taper transforms the SPP back to a photonic mode in the lower-right nanowire. **b**,**c**, Mode profiles of the SPP (**b**) and RF (**c**) signals, showing the colour-coded modulus of the complex electric-field vector.

[1]Institutes IPQ & IMT, Karlsruhe Institute of Technology (KIT), D-76131 Karlsruhe, Germany, [2]Institute of Electromagnetic Fields, ETH Zurich, 8092 Zurich, Switzerland, [3]Photonics Research Group, Ghent University-IMEC, 9000 Gent, Belgium, [4]GigOptix Inc., 8008 Zurich, Switzerland, [5]GigOptix Inc., Bothell, Washington 98011, USA. *e-mail: argishti.melikyan@kit.edu; wolfgang.freude@kit.edu; juergleuthold@ethz.ch

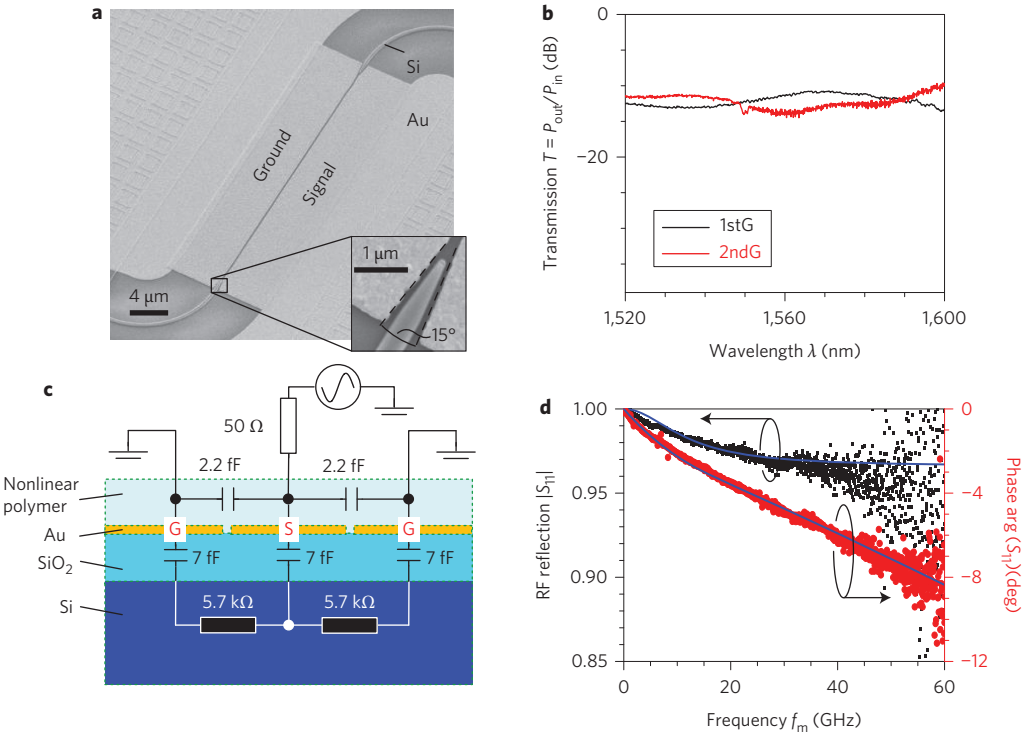

Figure 2 | Characteristics of fabricated PPMs. a, SEM image of the 1stG PPM (length, 34 µm). The image was taken before coating the sample with an electro-optic polymer. Lower-right inset: the clearly defined silicon nanowire taper, showing the good alignment of taper and slot. **b**, Comparison of the measured optical transmission of the 1stG device (black solid curve) with 2ndG modulators (red solid line) after coating with an electro-optic polymer, showing a flat transmission across a wide spectral range. **c**, Lumped element model of the 1stG modulator used for electrical characterization with a GSG probe. **d**, Magnitude and phase of the S_{11} RF reflection factor for frequencies up to 60 GHz. The modulus (left axis) and phase (right axis) of S_{11}, as calculated for the lumped element model depicted in **c**, are given as blue solid lines.

the compactness of a photonic-crystal modulator[8,14] and the energy efficiency of a ring modulator[3–7]. In particular, the reported PPM has an RF bandwidth that exceeds the bandwidth of known silicon modulators[3–15], while its footprint remains among the smallest[3–8,14].

Our PPM consists of two metal tapers that perform the photonic-to-plasmonic mode conversion and a phase modulator section located between them (Fig. 1a). The metal taper narrows with an angle of 15° and is used as an interface between the silicon photonics and plasmonics[30]. Light guided through the silicon nanowire efficiently excites the SPP via the metal taper. The SPP is then guided into the phase modulator section, which consists of two metal pads separated horizontally by a nanometre-scale vertical slot (Fig. 1b,c). The slot is filled with a nonlinear organic material, the refractive index n of which can be changed via the Pockels effect by applying a static electric field U/w_{gap} (modulating voltage U, gap width w_{gap}). With an electro-optic coefficient r_{33}, the change in the refractive index is equal to $\Delta n = (1/2) \times r_{33} n^3 U/w_{gap}$ (ref. 31). By modulating the refractive index of the polymer in the slot, the information is encoded in the phase of the SPP. At the end of the modulator section, the SPP is back-converted into a photonic mode.

Noble metals such as gold or silver exhibit negative dielectric permittivity below their plasma frequency. For such metals, the modulus of the permittivity at communication wavelengths is typically two orders of magnitude larger than the permittivity of the nonlinear polymer[32]. This large permittivity contrast at the metal–polymer interface results in an optical field enhancement in the slot (Fig. 1b). Moreover, both optical and modulating fields are strongly confined to the slot, resulting in a near-perfect overlap between the optical and RF signals (Fig. 1b,c). Consequently, the U_π voltage for a phase shift of π at a given device length L is small, leading to a small voltage–length product $U_\pi \times L$. Accordingly, a sub-50-µm PPM with a sufficient modulation index η (unit rad) becomes feasible. In our device, we make use of the Pockels effect in a nonlinear polymer, thereby avoiding the speed limitation typically associated with the carrier lifetime in plasma-effect-based injection-type modulators[3,6,10]. The high conductivity of the metal sheets and the small capacitance of the device result in an ultra-small RC time constant, which does not pose a practical speed limitation[3–15]. Furthermore, the lumped structure of our PPM avoids the bandwidth limitation caused by the walk-off of electrical and optical signals. The purely capacitive nature of the device and the small U_π also make it energy-efficient. Optical broadband operation of the PPM is ensured by the weak wavelength dependence of the nonlinear polymer, by the inherently broadband metallic slot waveguide and by the metallic tapers.

We fabricated two generations of PPM on an silicon-on-insulator (SOI) platform (Supplementary Section 1). The first generation (1stG) of PPM was fabricated in a ground–signal–ground (GSG) configuration with metallic slots with a length of 34 µm and a width of 140 nm on each side of the signal electrode. In the second-generation (2ndG) PPM, the slot width was reduced to 140 nm, and the length to 29 µm. The 2ndG device was designed to have a ground–signal (GS) configuration. A scanning electron microscope (SEM) image of the 1stG device is shown in Fig. 2a.

We measured the optical loss of the modulator section by taking an equal-length SOI strip waveguide as a reference. The fabricated PPMs show broadband optical transmission (Fig. 2b). The average total loss is 12 dB for both modulators. The electrical properties of the 1stG modulator were studied by investigating the S_{11} RF reflection factor. The cross-section of the device and its equivalent electrical circuit are provided in Fig. 2c. The RF reflection factor $|S_{11}|$ was measured to be greater than 95% across a 60 GHz frequency range

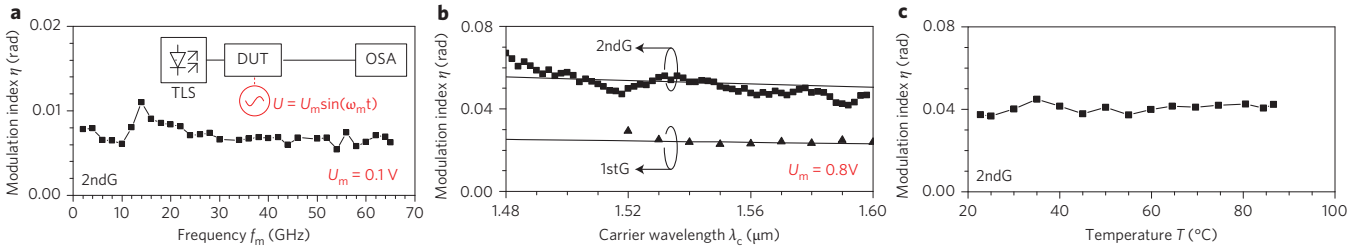

Figure 3 | Measured performance of the PPMs. a, Phase modulation index η versus RF frequency f_m for the 2ndG modulator. The frequency response is flat at least up to 65 GHz. Inset: experimental set-up used to measure η for various RF frequencies and carrier wavelengths. Infrared light from the tunable laser source (TLS) is sent to the device under test (DUT). The modulator is driven by a sinusoidal electrical signal with amplitude U_m, and the optical spectrum is measured at the output of the chip with an optical spectrum analyser (OSA). **b**, Modulation index for 1stG and 2ndG modulators versus optical carrier wavelength in a range of 120 nm for a modulation frequency of $f_m = 45$ GHz. The modulation index is essentially flat with respect to the carrier wavelength in this 120 nm range. Solid lines give the modulation index predicted by first-order perturbation theory. **c**, Thermal stability of the device tested for temperatures up to 85 °C. The polymer exhibits no degradation in its electro-optic coefficient at high temperatures, as has been shown elsewhere[30].

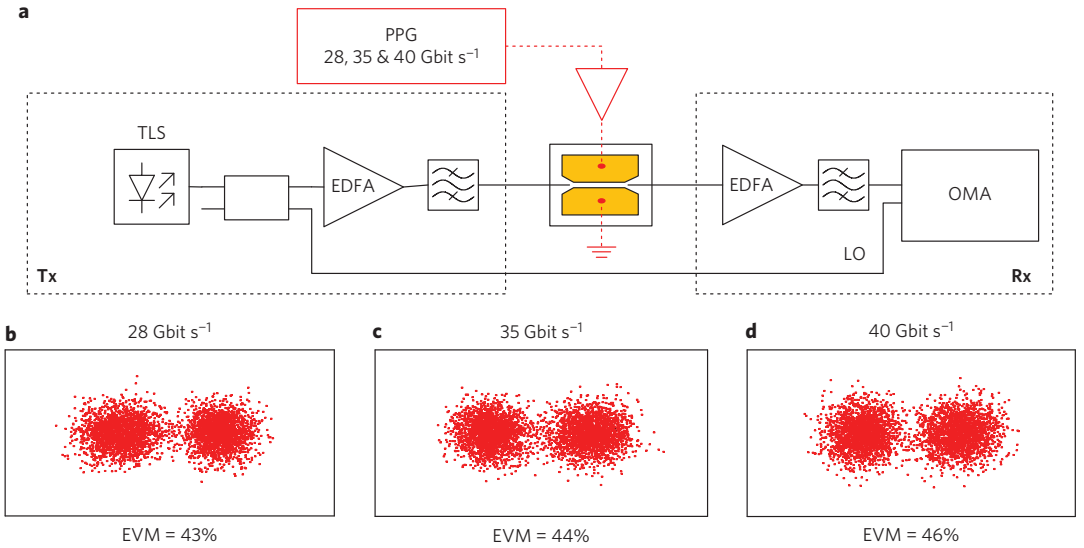

Figure 4 | Modulation experiments with the 1stG PPM. a, Experimental set-up for measuring the BER and EVM of a BPSK signal. Light with a wavelength of 1,550.92 nm is amplified by an erbium-doped fibre amplifier (EDFA), filtered, and sent to the DUT, wherein the phase of the SPP is modulated by the electrical RF signal. The resulting optical BPSK signal was detected with an Agilent optical modulation analyser (OMA). **b**–**d**, Constellation diagrams of the received BPSK signal for data rates 28 Gbit s^{-1}, 35 Gbit s^{-1} and 40 Gbit s^{-1}. EVMs between 43% and 46% are specified at the bottom of the graphs and correspond to BERs of 3×10^{-3} to 7×10^{-3}.

(Fig. 2d). We fit the measured electrical reflection factor with a lumped equivalent circuit (Fig. 2c) and found that the capacitance of each of the metallic slots is $C_{1stG} \approx 2.2$ fF. By geometrically scaling with respect to the slot width (140 nm versus 200 nm) and length (29 μm versus 34 μm), we estimate the capacitance of the 2ndG modulator to be $C_{2ndG} \approx 2.7$ fF.

We characterized the electro-optic frequency response of the modulators using the measurement set-up shown in the inset to Fig. 3a. The modulators are driven with a sinusoidal RF signal with an amplitude of U_m, and the resulting modulation index is measured (Supplementary Section 1). The measured phase modulation index for the 2ndG modulator is shown in Fig. 3a as a function of the RF modulation frequency up to 65 GHz. To cover the entire RF frequency range of the driver we selected a relatively small driving voltage amplitude of $U_m = 0.1$ V. The device exhibits an ultra-flat frequency response up to at least 65 GHz. Such a flat response was only possible due to the instantaneous Pockels effect and the ultra-small *RC* time constant of the device. To characterize the optical response we measured the phase modulation index for various carrier wavelengths λ_c, keeping the modulation frequency at 45 GHz and the driving voltage amplitude $U_m = 0.8$ V constant. Figure 3b shows the results for λ_c between 1,480 nm and 1,600 nm. Fitting the measured modulation index η with the one predicted with first-order perturbation theory (Supplementary Section 2), we derive the achieved on-chip electro-optic coefficient of the polymer. The electro-optic coefficients obtained for the 1stG and 2ndG devices are $r_{33} = 13$ pm V^{-1} and $r_{33} = 21$ pm V^{-1}, respectively.

Even though the used nonlinear polymer has been tested previously in a high-temperature environment[33], we carried out a thermal stability test to further confirm the operation of the device under operation conditions such as found, for example, in telecommunications racks. The modulation index was measured for various sample temperatures up to 85 °C. No degradation of the modulation index was found (Fig. 3c).

To test the high-speed capabilities of the 1stG modulator we encoded a data stream with a bit rate of up to 40 Gbit s^{-1}, the maximum rate available in our laboratory. The phase of the SPP was encoded with a $2^{31} - 1$ long pseudo-random bit sequence (PRBS) with a voltage swing of $U_{pp} = 7.5$ V, resulting in a peak-to-peak phase modulation of 0.23 rad. The resulting binary phase shift keyed (BPSK) signal was received by a coherent receiver. The error vector magnitudes (EVM) for three different data rates are

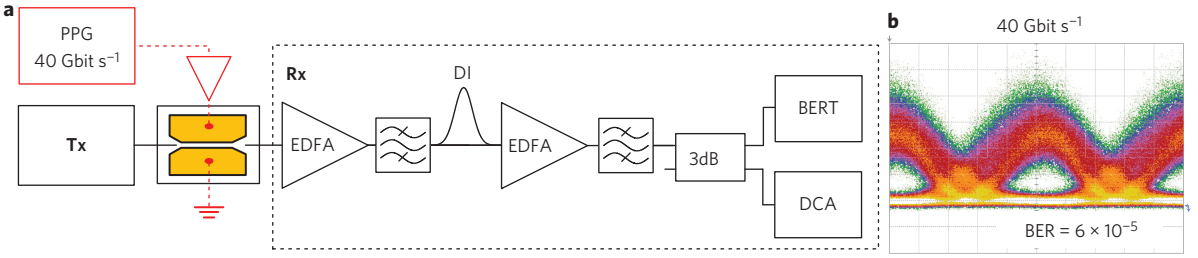

Figure 5 | Modulation experiments with the 2ndG PPM. a, Direct receiver set-up for detecting a BPSK signal. A 40 Gbit s^{-1} BPSK signal was converted to an intensity-modulated signal using a delay interferometer (DI) with a free spectral range of 40 GHz. To compensate for the losses of the in-house-built DI, the second preamplifier was added. A digital communication analyser (DCA) and bit error ratio tester (BERT) were used for eye diagram and BER measurements, respectively. **b**, Eye diagram of the received signal for a data rate of 40 Gbit s^{-1} and a corresponding BER of 6×10^{-5}.

provided in Fig. 4b–d. The bit error ratios (BERs) corresponding to the measured EVMs[34] are in the range of $(3–7) \times 10^{-3}$. The 2ndG modulator was encoded with a 40 Gbit s^{-1} data stream. In this case, the device was operated with an electrical signal with a reduced amplitude of $U_{pp} = 4.7$ V, resulting in a peak-to-peak phase modulation of 0.31 rad. This signal was subsequently converted into an intensity-modulated signal by means of a delay interferometer with a free spectral range (FSR) of 40 GHz (Fig. 5a). The signal was then detected directly with a single photodiode. A measured eye diagram with a BER of 6×10^{-5} is given in Fig. 5b. An optical physical link with such a BER can be used in both long- and short-range applications[35]. Taking into account the capacitance C_{2ndG} of the modulator we estimate an energy consumption per bit of $(2U_{pp})^2 \times C_{2ndG}/4 = 60$ fJ bit^{-1} for a voltage swing of $2U_{pp}$ across the device[36]. Using the latest electro-optic polymers[37], the average energy per bit could be reduced to 18 fJ bit^{-1} for a plasmonic Mach–Zehnder modulator (MZM) operating in push–pull, as we discuss in Supplementary Section 3.

In conclusion, we report the first successful experimental demonstration of a high-speed PPM. We demonstrate operation at a high bit rate of 40 Gbit s^{-1} for a device length of only 29 μm. The modulator exhibits a flat modulation frequency response up to at least 65 GHz. It can be operated across the whole optical *S*, *C* and *L*-bands. The thermal stability of the device for temperatures up to 85 °C has been assured. We believe that the concept has the potential to pave the way to future ultra-compact and CMOS-compatible on-chip Mach–Zehnder and in-phase and quadrature phase (IQ) plasmonic modulators such as needed to generate quadrature amplitude modulation formats.

Received 26 September 2013; accepted 8 January 2014; published online 16 February 2014

References

1. Reed, G. T., Mashanovich, G., Gardes, F. Y. & Thomson, D. J. Silicon optical modulators. *Nature Photon.* **4,** 518–526 (2010).
2. Leuthold, J. *et al.* Silicon–organic hybrid electro-optical devices. *IEEE J. Sel. Top. Quantum Electron.* **19,** 3401413 (2013).
3. Xu, Q., Schmidt, B., Pradhan, S. & Lipson, M. Micrometre-scale silicon electro-optic modulator. *Nature* **435,** 325–327 (2005).
4. Watts, M. & Trotter, D. Ultralow power silicon microdisk modulators and switches. *5th IEEE International Conference on Group IV Photonics* 4–6 (2008).
5. Dong, P., Liao, S., Feng, D., Liang, H. & Zheng, D. Low V_{pp}, ultralow-energy, compact, high-speed silicon electro-optic modulator. *Opt. Express* **17,** 22484–22490 (2009).
6. Baba, T. *et al.* 50-Gb/s ring-resonator-based silicon modulator. *Opt. Express* **21,** 11869–11876 (2013).
7. Thomson, D. J. *et al.* Self-aligned silicon ring resonator optical modulator with focused ion beam error correction. *J. Opt. Soc. Am. B* **30,** 445–449 (2013).
8. Nguyen, H. C., Hashimoto, S., Shinkawa, M. & Baba, T. Compact and fast photonic crystal silicon optical modulators. *Opt. Express* **20,** 22465–22474 (2012).
9. Liao, L. *et al.* 40 Gbit s^{-1} silicon optical modulator for high-speed applications. *Electron. Lett.* **43,** 1196–1197 (2007).
10. Green, W. M., Rooks, M. J., Sekaric, L. & Vlasov, Y. A. Ultra-compact, low RF power, 10 Gbit s^{-1} silicon Mach–Zehnder modulator. *Opt. Express* **15,** 17106–17113 (2007).
11. Thomson, D. J. *et al.* 50-Gb/s silicon optical modulator. *Photon. Technol. Lett.* **24,** 234–236 (2012).
12. Xiao, X. *et al.* High-speed, low-loss silicon Mach–Zehnder modulators with doping optimization. *Opt. Express* **21,** 4116–4125 (2013).
13. Ding, R. *et al.* Demonstration of a low $V_{\pi}L$ modulator with GHz bandwidth based on electro-optic polymer-clad silicon slot waveguides. *Opt. Express* **18,** 15618–15623 (2010).
14. Brosi, J. M. *et al.* High-speed low-voltage electro-optic modulator with a polymer-infiltrated silicon photonic crystal waveguide. *Opt. Express* **16,** 4177–4191 (2008).
15. Alloatti, L. *et al.* 42.7 Gbit s^{-1} electro-optic modulator in silicon technology. *Opt. Express* **19,** 11841–11851 (2011).
16. Raether, H. *Surface Plasmons on Smooth and Rough Surfaces and on Gratings* (Springer, 1988).
17. Maier, S. *Plasmonics: Fundamentals and Applications* (Springer, 2007).
18. Schuller, J. A. *et al.* Plasmonics for extreme light concentration and manipulation. *Nature Mater.* **9,** 193–204 (2010).
19. Gramotnev, D. K. & Bozhevolnyi, S. I. Plasmonics beyond the diffraction limit. *Nature Photon.* **4,** 83–91 (2010).
20. Kauranen, M. & Zayats, A. V. Nonlinear plasmonics. *Nature Photon.* **6,** 737–748 (2012).
21. Fang, Z. *et al.* Graphene–antenna sandwich photodetector. *Nano Lett.* **12,** 3808–3813 (2012).
22. Nikolajsen, T., Leosson, K. & Bozhevolnyi, S. I. Surface plasmon polariton based modulators and switches operating at telecom wavelengths. *Appl. Phys. Lett.* **85,** 5833–5835 (2004).
23. Schildkraut, J. Long-range surface plasmon electrooptic modulator. *Appl. Opt.* **27,** 4587–4590 (1988).
24. Cai, W., White, J. & Brongersma, M. Compact, high-speed and power-efficient electrooptic plasmonic modulators. *Nano Lett.* **9,** 4403–4411 (2009).
25. Randhawa, S. *et al.* Performance of electro-optical plasmonic ring resonators at telecom wavelengths. *Opt. Express* **20,** 2354–2362 (2012).
26. Dionne, J. A., Diest, K., Sweatlock, L. A. & Atwater, H. A. PlasMOStor: a metal–oxide–Si field effect plasmonic modulator. *Nano Lett.* **9,** 897–902 (2009).
27. Melikyan, A. *et al.* Surface plasmon polariton absorption modulator. *Opt. Express* **19,** 8855–8869 (2011).
28. Sorger, V. J., Lanzillotti-Kimura, N. D., Ma, R.-M. & Zhang, X. Ultra-compact silicon nanophotonic modulator with broadband response. *Nanophotonics* **1,** 17–22 (2012).
29. Feigenbaum, E., Diest, K. & Atwater, H. A. Unity-order index change in transparent conducting oxides at visible frequencies. *Nano Lett.* **10,** 2111–2116 (2010).
30. Pile, D. F. P. & Gramotnev, D. K. Adiabatic and nonadiabatic nanofocusing of plasmons by tapered gap plasmon waveguides. *Appl. Phys. Lett.* **89,** 041111 (2006).
31. Boyd, R. W. *Nonlinear Optics* (Academic, 2008).
32. Johnson, P. & Christy, R. Optical constants of the noble metals. *Phys. Rev. B* **6,** 4370–4379 (1972).
33. Jin, D. *et al.* EO polymer modulators reliability study. *Proc. SPIE Org. Photon. Mater. Dev. XII* **7599,** 75990H (2010).
34. Schmogrow, R. *et al.* Error vector magnitude as a performance measure for advanced modulation formats. *IEEE Photonic. Tech. Lett.* **24,** 61–63 (2012); *correction* **24,** 2198 (2012).
35. Zheng, X. *et al.* Energy-efficient error control for tightly coupled systems using silicon photonic interconnects. *J. Opt. Commun. Netw.* **3,** A21 (2011).
36. Miller, D. A. B. Energy consumption in optical modulators for interconnects. *Opt. Express* **20,** A293–A308 (2012).

37. Palmer, R. *et al.* High-speed silicon-organic hybrid (SOH) modulator with 1.6 fJ bit^{-1} and 180 pm V^{-1} in-device nonlinearity, in *ECOC London 2013*, paper We3B3.

Acknowledgements
The authors acknowledge support from EU research projects NAVOLCHI and SOFI, the Helmholtz International Research School for Teratronics (HIRST), the Karlsruhe School of Optics & Photonics (KSOP), the Center for Functional Nanostructures (CFN), the German Research Foundation (DFG) and Karlsruhe Nano Micro Facility (KNMF). Silicon-on-insulator waveguides were fabricated by IMEC in the framework of ePIXfab.

Author contributions
A.Me. developed the concept, designed and fabricated the modulators, performed the experiments, analysed the data and wrote the paper. L.A. built the poling equipment, and developed the poling procedure and the experimental method to estimate the modulation index. D.H., P.C.S., J.L. and R.P. performed the experiments. D.K. helped in designing the passive silicon platform. B.C. and R.D. developed and synthesized the M3 nonlinear polymer. A.Mu., D.V.T. and M.S. provided support in fabrication. M.K., C.K., W.F. and J.L. developed the concept, designed the experiment and wrote the manuscript.

Additional information
Supplementary information is available in the online version of the paper. Reprints and permissions information is available online at www.nature.com/reprints. Correspondence and requests for materials should be addressed to A.M., W.F. and J.L.

Competing financial interests
The authors declare no competing financial interests.